A geometric defect marker predicts transport classes in directed photonic meshes

Ahmed Alayar[1]
[1] *Independent Researcher, Kuwait*
(Dated: February 1, 2026)

Passive photonic meshes are attractive for low-latency analog processing, yet scalable coherent architectures often require phase stabilization and tight timing control. We study a complementary operating point: layered directed photonic meshes operated in an incoherent intensity-transport regime, where macroscopic output statistics are governed by topology rather than phase-coherent interference. We introduce a topology-only geometric defect marker Δa^*, defined as the mismatch between robust (Theil–Sen) and least-squares fixed points of a coarse-grained curvature–branching response measured on the condensation DAG of the mesh topology. Across ensemble sweeps and two system sizes, Δa^* predicts a crossover in channel participation n_{eff}/W, separating bulk-like transport ($\Delta a^* \approx 0$, low participation) from defect-mediated mixing ($\Delta a^* \lesssim -0.2$, higher participation). Crucially, this separation persists when the injection site is fixed in the bulk interior for both pristine and knotted topologies, isolating geometry from boundary-proximity artifacts. We further show that increasing defect strength (knot coupler density p_{knot}) tunes n_{eff}/W continuously, and we verify that integrated and distributional outputs are insensitive to injection timing jitter up to 50 ps, consistent with clock-tolerant incoherent operation. These results provide a reproducible geometry→transport dictionary for defect-enabled photonic mixing networks.

Introduction. Photonic integrated circuits enable fast, low-energy linear transforms and analog computing, but scalable coherent meshes often pay substantial overhead in calibration, phase stabilization, and timing distribution [1–5]. A complementary regime is to operate in incoherent intensity transport, where detectors integrate optical energy and the relevant observables are insensitive to relative phase. In this regime, the design question shifts from *phase programming* to *topology selection*: which directed mesh topologies realize narrow, waveguide-like transport versus distributed mixing in the bulk?

Here we provide a compact, topology-only answer for a standard directed mesh model with a localized high-connectivity defect (a "knot"). We show that a single geometric marker, Δa^*, computed from a coarse-grained response on the condensation DAG of the topology, predicts the transport class. We emphasize that the observed separation is not a claim of critical-exponent universality; rather, it is a size-robust classification of transport regimes by a coarse geometric coordinate.

Directed intensity transport. We consider a layered mesh with W parallel channels and L propagation stages. At each stage, candidate 2×2 couplers between adjacent channels are present with bulk probability p_f. A localized knot defect is embedded by raising the coupler probability to p_{knot} inside a compact layer–channel region (here: channels 6–14 and layers 10–18 for W=20, L=50; channels 9–19 and layers 14–26 for W=28, L=70). Transport in the incoherent regime is modeled by nonnegative mixing of intensities,

$$x^{(\ell+1)} = T_\ell x^{(\ell)}, \qquad y = x^{(L)}, \tag{1}$$

where $x^{(\ell)} \in \mathbb{R}^W_{\geq 0}$ and T_ℓ encodes coupler placement and splitting at stage ℓ. We quantify the output distribution y using (i) contrast $C \equiv y_{\max}/\bar{y}$ and (ii) an effective number of populated outputs $n_{\mathrm{eff}} \equiv \exp(H)$, where $H = -\sum_i p_i \ln p_i$ is the Shannon entropy of $p_i = y_i / \sum_j y_j$ [6]. For cross-size comparisons we report the participation fraction n_{eff}/W.

Condensation-DAG geometry and defect marker. Given the directed mesh graph, we compute strongly connected components and contract them to form the condensation DAG [7]. On the condensation DAG, for SCC nodes X define a one-step future-cone volume $V(X) = 1 + |N^+(X)|$ and an edge-level cone-growth proxy

$$\kappa(X \to Y) = V(Y) - V(X) \tag{2}$$

for edges $X \to Y$. As a local branching observable define $\rho(X) = \deg^+(X) - 1$. At a coarse scale R we block the condensation DAG into many depth-local blocks of size $\sim R$, compute block averages (κ_R, ρ_R), and fit an affine response across blocks,

$$\kappa_R \simeq a_R \rho_R + b_R. \tag{3}$$

We estimate (a_R, b_R) by least squares (LS) and by a robust Theil–Sen line fit [8, 9]. A scaling window is identified algorithmically as a plateau of a_R at the largest accessible R; the fixed point a^* is taken as the median slope over this plateau. We then define the defect marker as the estimator mismatch

$$\Delta a^* \equiv a^*_{\mathrm{rob}} - a^*_{\mathrm{LS}}. \tag{4}$$

Intuitively, in bulk-like substrates the block scatter in Eq. (3) is close to affine with modest noise, and LS and robust slopes coincide ($\Delta a^* \approx 0$). A localized defect introduces a small set of leverage/outlier blocks in the (κ_R, ρ_R) relation, shifting the LS slope while leaving the robust slope comparatively stable; Δa^* thus quantifies

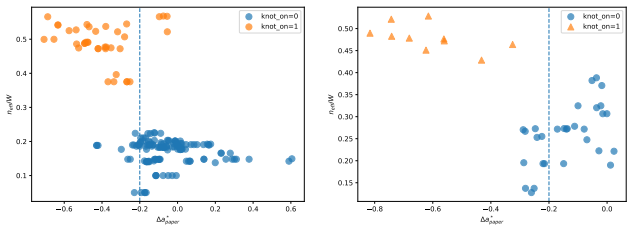

FIG. 1. **Geometry→transport dictionary.** Participation fraction n_{eff}/W versus defect marker Δa^*. Left: $W{=}20, L{=}50$ selection comparing an edge-guided reference (knot off, injection at channel 0) to a defect-enabled operating point (knot on, interior injection at channel 9). Right: fixed interior-injection control at a larger size ($W{=}28, L{=}70$) with injection fixed at channel 14 for both knot-off and knot-on instances. Across sizes and boundary conditions, bulk-like transport clusters near $\Delta a^* \approx 0$, while defect-mediated mixing shifts to $\Delta a^* \lesssim -0.2$ with higher participation.

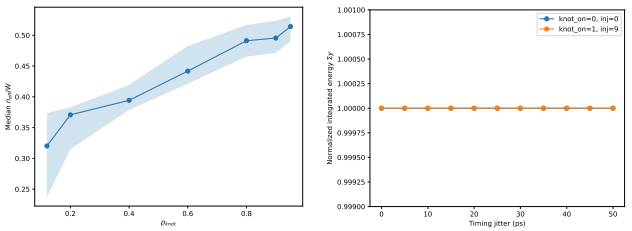

FIG. 2. **Control knobs and clock tolerance.** (a) Continuous tuning of participation by defect strength: median n_{eff}/W increases monotonically with knot coupler density p_{knot} (sweep at fixed $W{=}20, L{=}50, p_f{=}0.12$, interior injection). (b) Timing tolerance in pulsed mode: normalized integrated output energy versus injection timing jitter (0–50 ps) is invariant for both a bulk reference and a defect-mediated operating point (within numerical precision).

the geometric relevance of the defect at coarse scale. Importantly, Δa^* is computed from topology alone and does not use transport data.

Results: a geometry→transport dictionary. Figure 1 shows the main result: Δa^* predicts transport class via a one-dimensional relationship with participation. For a base ensemble ($W{=}20, L{=}50$), an edge-guided reference (knot absent, injection at channel 0) clusters near $\Delta a^* \approx 0$ with low participation, while a defect-enabled operating point (knot present, interior injection at channel 9) shifts to more negative Δa^* and higher n_{eff}/W. Quantitatively, the medians shift from $(\Delta a^*, n_{\text{eff}}/W) = (-0.087, 0.184)$ (knot off) to $(-0.403, 0.491)$ (knot on). To disentangle defect geometry from boundary proximity, we perform a fixed interior-injection control at a larger size ($W{=}28, L{=}70$) where both knot-off and knot-on instances are injected at the same mid-channel (channel 14). The separation persists with medians $(-0.139, 0.271)$ (knot off) versus $(-0.619, 0.477)$ (knot on), and the transition band lies around $\Delta a^* \approx -0.25$ (Fig. 1). As a compact predictive summary, using Δa^* as a single-feature classifier for the defect-enabled class yields ROC AUC 0.93 (W=20 selection) and 1.00 (fixed-injection replicate) on plateau-valid instances (Fig. S2). Plateau selection itself does not produce a spurious separation: in the W=20 selection the plateau-valid fraction is 0.92 (knot off) versus 0.27 (knot on), and excluded knot-on instances have similarly high participation (Fig. S6).

Continuous control and clock tolerance. The defect marker suggests a design knob: increasing defect strength should move the system along the participation curve. Figure 2(a) confirms this by sweeping the knot coupler density p_{knot} at fixed (W, L, p_f), showing a monotone increase in median n_{eff}/W. We also verify timing tolerance in a pulsed injection mode by introducing injection timing jitter up to 50 ps and measuring integrated outputs. Figure 2(b) shows that normalized integrated output energy is invariant across the jitter window for both a bulk reference and a defect-mediated operating point. In our implementation, distributional observables (participation and contrast) are likewise invariant across 0–50 ps (Fig. S7), consistent with incoherent detection and validating the use of integrated, clock-tolerant observables for transport classification.

Discussion. We introduced a simple, reproducible geometric marker on the condensation DAG of a directed mesh topology and showed that it predicts whether the mesh realizes bulk-like or defect-mediated mixing in an incoherent intensity-transport regime. The key implication is a topology-only geometry→transport surrogate: it does not fit microscopic phases and does not require simulating full wave interference. The present study is numerical and uses an idealized directed mixing model; incorporating additional photonic nonidealities (loss, fabrication disorder, backscattering) and experimental validation are important next steps. Notably, uniform multiplicative loss (a per-stage scalar attenuation) cancels in normalized observables and therefore does not change n_{eff}/W; the relevant open question is robustness to *nonuniform* attenuation and weak backward coupling. Nevertheless, because Δa^* is defined on coarse-grained topological structure and exhibits strong classifier-quality under fixed interior injection, it is a natural candidate for design heuristics and for compiler constraints in defect-enabled photonic mixing networks.

Data and code availability. All scripts, configurations, and processed datasets required to reproduce the figures in this Letter and the Supplemental Material are available at github.com/a7midi/PTPP.

[1] M. Reck, A. Zeilinger, H. J. Bernstein, and P. Bertani, "Experimental realization of any discrete unitary opera-

tor," *Phys. Rev. Lett.* **73**, 58 (1994).

[2] W. R. Clements, P. C. Humphreys, B. J. Metcalf, W. S. Kolthammer, and I. A. Walmsley, "Optimal design for universal multiport interferometers," *Optica* **3**, 1460 (2016).

[3] D. A. B. Miller, "Self-configuring universal linear optical component," *Photonics Research* **1**, 1 (2013).

[4] D. Vandoorne *et al.*, "Experimental demonstration of reservoir computing on a silicon photonics chip," *Nat. Commun.* **5**, 3541 (2014).

[5] A. N. Tait *et al.*, "Neuromorphic photonic networks using silicon photonic weight banks," *Sci. Rep.* **7**, 7430 (2017).

[6] C. E. Shannon, "A mathematical theory of communication," *Bell Syst. Tech. J.* **27**, 379 (1948).

[7] R. E. Tarjan, "Depth-first search and linear graph algorithms," *SIAM J. Comput.* **1**, 146 (1972).

[8] H. Theil, "A rank-invariant method of linear and polynomial regression analysis," *Nederl. Akad. Wetensch. Proc. Ser. A* **53**, 386 (1950).

[9] P. K. Sen, "Estimates of the regression coefficient based on Kendall's tau," *J. Am. Stat. Assoc.* **63**, 1379 (1968).